HHS Public Access

Author manuscript

Nanotoxicology. Author manuscript; available in PMC 2019 November 01.

Published in final edited form as:

Nanotoxicology. 2018 November ; 12(9): 975–991. doi:10.1080/17435390.2018.1502830.

Role of p53 in the Chronic Pulmonary Immune Response to Tangled or Rod-Like Multi-Walled Carbon Nanotubes

Katherine S. Duke[1], **Elizabeth A. Thompson**[1], **Mark D. Ihrie**[1], **Alexia J. Taylor-Just**[1], **Elizabeth A. Ash**[2], **Kelly A. Shipkowski**[1], **Jonathan R. Hall**[1], **Debra A. Tokarz**[2], **Mark F. Cesta**[3], **Ann F. Hubbs**[4], **Dale W. Porter**[4], **Linda M. Sargent**[4], and **James C. Bonner**[1,*]

[1]Toxicology Program, Department of Biological Sciences, North Carolina State University, Raleigh, NC 27606

[2]College of Veterinary Medicine, North Carolina State University, Raleigh, NC 27606

[3]National Institute of Environmental Health Sciences, Research Triangle Park, NC 27709

[4]National Institute for Occupational Safety and Health, Morgantown, WV 26505

Abstract

The fiber-like shape of multi-walled carbon nanotubes (MWCNTs) is reminiscent of asbestos, suggesting they pose similar health hazards when inhaled, including pulmonary fibrosis and mesothelioma. Mice deficient in the tumor suppressor p53 are susceptible to carcinogenesis. However, the chronic pathological effect of MWCNTs delivered to the lungs of p53 heterozygous ($p53^{+/-}$) mice has not been investigated. We hypothesized that $p53^{+/-}$ mice would be susceptible to lung tumor development after exposure to either tangled (t-) or rod-like (r-) MWCNTs. Wild type ($p53^{+/+}$) or $p53^{+/-}$ mice were exposed to MWCNTs (1 mg/kg) via oropharyngeal aspiration weekly over 4 consecutive weeks and evaluated for cellular and pathologic outcomes 11-months post initial exposure. No lung or pleural tumors were observed in $p53^{+/+}$ or $p53^{+/-}$ mice exposed to either t- or rMWCNTs. In comparison to tMWCNTs, the rMWCNTs induced the formation of larger granulomas, a greater number of lymphoid aggregates and greater epithelial cell hyperplasia in terminal bronchioles in both $p53^{+/-}$ and $p53^{+/+}$ mice. A constitutively larger area of CD45R

*Corresponding author: Dr. James C. Bonner, jcbonner@ncsu.edu.

Authors contributions

JCB, KSD, and EAT conceived and planned the experiments. JCB, KSD, EAT, KAS, EAA, MDI, KAS, AJT carried out the experiments and quantitative analysis. JCB, KSD, DAT, JRH, MFC, AFH, DWP, and LMS contributed to the interpretation of the results. KSD took the lead in writing the manuscript. All authors provided critical feedback and helped shape the research, analysis and manuscript.

DECLARATIONS

Ethics approval and consent to participate:

Ethics approval for animal use was given by the North Carolina State University IACUC.

Consent for publication

Not applicable

Availability of data and material

All data generated or analyzed during this study are included in this published article and its supplementary information files.

Competing interests

The authors declare that they have no competing interests.

DISCLAIMER

The findings and conclusions in this report are those of the authors and do not necessarily represent the views of the National Institute for Occupational Safety and Health.

$^{+}$/CD3^{+} lymphoid tissue was observed in p53$^{+/-}$ mice compared to p53$^{+/+}$ mice. Importantly, p53$^{+/-}$ mice had larger granulomas induced by rMWCNTs as compared to p53$^{+/+}$ mice. These findings indicate that a combination of p53 deficiency and physicochemical characteristics including nanotube geometry are factors in susceptibility to MWCNT-induced lymphoid infiltration and granuloma formation.

Keywords

Caron nanotubes; immunotoxicology; cancer; granuloma; p53

INTRODUCTION

The commercial use and incorporation of carbon nanotubes (CNTs) into consumer products has been on the rise because of their unique optical, electrical and magnetic properties (Kuick Research, 2017); however, little is known about the risks of possible exposure to these materials. Multi-walled carbon nanotubes (MWCNTs) possess some characteristics that are similar to asbestos, a known human carcinogen. For example, MWCNTs have a fiber-like shape and contain trace metal catalysts (e.g., Fe, Ni) from the manufacturing process (Poland et al, 2008). Physicochemical characteristics of MWCNTs, including their high aspect ratio, durability, biological persistence, rigidity and their ability to create chromosomal abnormalities are shared with asbestos and could influence their carcinogenic and fibrogenic potential (Siegrist et al 2014; Nagai et al., 2011; Barrett et al., 1989; Hubbs et al., 2011).

There is concern that MWCNTs might behave like asbestos, which has been shown to cause pulmonary fibrosis and mesothelioma in humans and animal models. Like asbestos, MWCNTs delivered to the lungs of mice cause pulmonary fibrosis and lung cancer (Porter et al., 2010; Sargent et al., 2014). MWCNTs delivered to the lungs of mice by inhalation also cause interstitial, airway and sub-pleural fibrosis but not granulomas (Ryman-Rasmussen et al., 2009b), whereas oropharyngeal aspiration causes both pulmonary fibrosis and granuloma formation (Muller et al., 2005; Dong et al., 2014; Duke et al., 2017). MWCNTs also reach the pleura of mice after inhalation or aspiration and cause inflammatory lesions at the mesothelial lining and proliferation of mesothelial cells (Ryman-Rasmussen et al., 2009a; Xu et al., 2012; Mercer et al., 2013). Increased promotion of adenocarcinomas was reported in mice that were first exposed to the tumor initiator methylcholanthrene (MCA) followed by exposure to rod-like MWCNTs (Sargent et al., 2014). That study also showed serosal tumors morphologically consistent with sarcomatous mesotheliomas in five mice co-exposed to MCA and MWCNTs and in one mouse from the MCA control treatment group, but none resulting from MWCNT exposure alone.

There is some evidence to support the development of MWCNT-induced mesothelioma in rodent models. The administration of fibers by intraperitoneal (i.p.) injection in mice has been used as a surrogate to test mesothelioma development from the mesothelial cells on serosal surfaces. Administration of MWCNTs or asbestos to rodents by i.p. injection has also been shown to cause granuloma or mesothelioma on the lining of the abdominal cavity

(Poland et al., 2008; Takagi et al., 2008). Mesothelioma formation has been shown one year post i.p. injection of MWCNTs in tumor-susceptible heterozygous mice lacking one allele of the tumor suppressor p53 ($p53^{+/-}$); however, no comparison was done to wild type p53 mice ($p53^{+/+}$) (Takagi et al., 2012). Mesothelioma has also been demonstrated in wild type rats one and two years after MWCNT exposure by i.p. injection (Nagai et al., 2011; Rittinghausen et al., 2014). Furthermore, intrascrotal injection of MWCNTs has been shown to induce mesotheliomas in rats at time points shorter than one year following exposure (Sakamoto et al., 2009). There is little evidence for pleural mesothelioma in rodents by direct pulmonary exposure. Inhalation of rod-like MWCNTs in Fisher 344 (F344) rats induced lung cancer but not mesothelioma (Kasai et al., 2016), while intratracheal instillation of MWCNTs in F344 rats induced lung tumors and mesothelioma (Suzui et al., 2016). Inhaled MWCNTs reach the pleural space and are highly retained, thus having the potential to induce sustained pleural inflammation, mesothelial injury and progressive subpleural fibrosis at this location (Ryman-Rasmussen et al., 2009a; Murphy et al., 2013; Xu et al., 2014). However, the lack of evidence for mesothelioma in many mouse studies after MWCNT exposure may be due the relative resistance of some mouse strains or due to different physicochemical features of MWCNT products. For example, one rod-like MWCNT product has been classified as having greater potential for carcinogenicity in humans compared to other MWCNTs (IARC 2017).

Genetic alterations also play a part in the development of pulmonary diseases like lung cancer, mesothelioma and fibrosis. The p53 tumor suppressor plays a key role in the regulation of the pulmonary carcinogenic and fibrotic processes by controlling cellular responses to stress including DNA repair, apoptosis and cell cycle progression (Dai et al., 2010). p53 plays a particularly important role in controlling cell proliferation (Agarwal et al., 1995). Mutation of either *p53* allele can lead to loss of both function and proliferation control, potentially resulting in fibrosis or cancer (Zilfou and Lowe, 2009). Some disease states are associated with alteration of p53; for example, samples taken from patients with idiopathic pulmonary fibrosis (IPF) have high *p53* mutation incidences (Takahashi et al., 2002; Vancheri et al., 2010). Furthermore, the majority of IPF patients with overexpression of p53 have been found to have multiple point mutations in the *p53* gene (Hojo et al., 1998). Subchronic exposure (12 weeks) of transformed human lung epithelial cells to single walled CNTs *in vitro* resulted in neoplastic marker development and resistance to apoptosis via decreased p53 activation (Wang et al., 2011a). Knock-down or knock-out of *p53* can increase tumor incidence and burden associated with decreased life span of the genetically modified mice (Wang et al., 2006; Wang et al., 2011b; Xu et al., 2014). p53 also plays a role in IL-17-induced tumor cell growth (Xu et al., 2014). In addition, p53 acts cooperatively with NFkB to drive proinflammatory cytokine production (Lowe et al., 2014). Therefore, p53 is a crucial regulator of cellular homeostasis, and alterations of *p53* may result in the promotion of disease states in the lung.

To our knowledge, no studies have shown that direct pulmonary exposure of mice to MWCNTs, either by inhalation or oropharyngeal aspiration, results in mesothelioma in the absence of a tumor initiator. Additionally, despite the demonstrated role of p53 in pulmonary disease states, including carcinogenesis and fibrosis, the role of p53 in MWCNT-induced pulmonary pathology has not been investigated. We hypothesized that p53-deficient mice

would be susceptible to fibrosis or cancer following chronic exposure to MWCNTs. To evaluate the influence of physicochemical characteristics with emphasis on nanotube geometry, both tangled (t-) and rod-like (r-) MWCNTs were utilized for this study. Heterozygous p53-deficient ($p53^{+/-}$) mice were exposed to tMWCNTs or rMWCNTs via oropharyngeal aspiration and lung pathology was assessed 11 months post-initial exposure. While mesothelioma was not observed in $p53^{+/-}$ mice exposed to either tMWCNTs or rMWCNTs, we discovered that $p53^{+/-}$ mice were susceptible to MWCNT-induced granuloma formation and the formation of tertiary lymphoid tissue in lung tissue. Moreover, rMWNCTs caused significantly larger granulomas compared to tMWCNTs in wild type ($p53^{+/+}$) mice and $p53^{+/-}$ mice.

METHODS

Nanomaterial Preparation.

tMWCNTs were purchased from Helix Material Solutions Inc., (Richardson, TX) and were characterized previously (Ryman-Rasmussen et al., 2009a). rMWCNTs (XNRI MWCNT-7 05072001 K28) were manufactured by Mitsui & Co (Tokyo, Japan) and obtained from NIOSH. The MWCNTs used in this study have been previously characterized for residual trace metal content, diameter, length, surface area, zeta potential and static bending ratio as an index of rigidity (Ryman-Rasmussen et al., 2009b; Porter et al., 2010; Mercer et al., 2011; Hilton et al., 2016; Duke et al., 2017). A summary of physicochemical characteristics of tMWCNT and rMWCNT is shown in Supplemental Table 1. MWCNTs were prepared in 0.1% Pluronic F-68 Solution (#P5556) from Sigma (Saint Louis, MO) and diluted with Dulbecco's phosphate-buffered saline (DPBS).

Animal Care.

Pathogen-free wild type and $p53^{+/-}$ mice bred from a C57BL/6 background were purchased from The Jackson Laboratory (Bar Harbor, ME). Mice were housed in an IACUC-approved and AALAC-accredited animal facility. Animals were housed 1-5 per cage and fed LabDiet 5001 rodent diet and water *ad libitum*. All animal procedures were approved by the North Carolina State University IACUC.

Dosing of Mice.

Wild type and $p53^{+/-}$ mice aged 8-12 weeks were dosed once a week for 4 weeks with 1 mg/kg tMWCNTs or rMWCNTs in 0.1% pluronic surfactant solution by oropharyngeal aspiration (OPA) under isoflurane anesthesia. The cumulative dose of 4 mg/kg achieved by the four consecutive OPA doses of MWCNTs was chosen based on other previous studies (Porter et al., 2010; Sargent et al., 2014). Control mice received an equivalent dose volume of the vehicle, 0.1% Pluronic surfactant solution. The control wild type groups contained N=10, the wild type tMWCNT exposed group contained N=10, the wild type rMWCNT exposed group N=8, the $p53^{+/-}$ control group N=14, the $p53^{+/-}$ tMWCNT exposed group N=9, and the $p53^{+/-}$ rMWCNT exposed group N=8. The dosing strategy and animal numbers are summarized in Supplemental Fig. 1.

Necropsy and Collection of Samples.

Mice were euthanized utilizing pentobarbital fatal injection 11 months post-initial exposure to tMWCNTs, rMWCNTs, or vehicle. Only two mice from the $p53^{+/-}$ rMWCNT group did not survive the entirety of the study, one died following the 4th and final dose and the other was euthanized due to the development of a debilitating sarcoma. Furthermore, two $p53^{+/-}$ mice, one exposed to tMWCNT and the other to rMWCNT, were excluded from analysis due to MWCNT-independent development of adenocarcionoma and alveolar proteinosis, respectively. Two 0.5 mL aliquots of DPBS were lavaged to collect bronchoalveolar lavage fluid (BALF) for cytokine and cellular content. The left lobe of the lung was inflated with approximately 500 μL neutral buffered formalin (Azer Scientific, Morgantown, PA) and fixed overnight, dehydrated in 70% ethanol overnight, then embedded in paraffin for histology and the right lobes were divided equally into RNAlater (Fisher Scientific, Waltham, MA) or snap frozen in a cryotube for mRNA and protein analysis, respectively.

Bromodeoxyuridine (BrdU) Immunohistochemical Staining (IHC).

To label cells actively synthesizing DNA, intraperitoneal injections of 100 mg/kg BrdU (Sigma, Saint Louis, MO) in DPBS were administered to mice one-hour prior to euthanasia. Lungs and small intestine (positive control) were sectioned at 5 μm using a microtome, mounted on a negatively charged slide and stained using a protocol described previously (Duke et al., 2017).

Pleural Lesion Analysis.

Three lung sections from each mouse were cut and stained with H&E. The visceral pleura was carefully evaluated for inflammatory, fibrotic or carcinogenic lesions in all sections consistent with our previous analysis of pleural lesions after MWCNT OPA in C57BL/6 mice (Ryman-Rasmussen et al., 2009a).

Granuloma Analysis.

Trichrome-stained lung sections containing granulomas were imaged with a respective scale bar. Each granuloma was characterized by both the presence of MWCNTs in the tissue and an associated inflammatory reaction to them consisting of epithelioid macrophages and/or fibrosis. The presence of MWCNTs within alveolar macrophages with no associated fibrosis or epithelioid macrophages was not considered a granuloma. Adobe Photoshop CS5 was utilized to measure granuloma area by using the ruler tool to measure and set a custom measurement scale by converting pixels to micrometers (μm). The lasso tool was used to encompass the granuloma. A granuloma was defined as a mass of cells (mainly epithelioid macrophages) surrounding a foreign body. Each granuloma area was measured using Photoshop software and tracing around the easily defined border excluding surrounding epithelial cells (Schneider et al., 2012). Total lung section area was measured by first combining lung images using the image stitching plugin available through Fiji (Preibisch et al., 2009). The area of the lung was then measured using the lasso tool after being set to the dimensions of the image.

Lymphoid Tissue Quantification Analysis.

Three lung sections from each mouse were cut, stained with bromodeoxyuridine (BrdU) and analyzed for inducible bronchus-associated lymphoid tissue (iBALT) or ectopic lymphoid tissue (ELT) formations by scanning these sections for lymphoid structures. Each iBALT or ELT identified was imaged and the area was measured using the lasso tool in Photoshop from BrdU IHC-stained slides. Total lung section area was measured from BrdU IHC stained mouse lungs that were imaged at 40X and stitched together using the ImageJ stitching plugin in Fiji (Preibisch et al., 2009). The total lung section area was quantitatively measured in ImageJ as were all lymphoid aggregates of more than 10 mononuclear cells. These were put into categories of iBALT or ELT for further analysis. The total number of iBALT or ELT formations and the number containing BrdU positive cells were counted. The number of granulomas adjacent to lymphoid tissue were also counted using the H&E stained sections.

Lymphoid Tissue Characterization.

Three lung tissue blocks from each genotype and treatment group were selected for IHC staining of a T cell marker, CD3, and a pan B cell marker, CD45R/B220, to assess lymphoid tissue structure.

Hyperplasia Analysis at First Terminal Bronchial Duct Bifurcation.

Images were taken at 100X of the first bronchial duct bifurcation from BrdU immunohistochemically-stained lung sections. These images were centered to keep imaging consistent; some mouse lungs did not have these structures in the sections, thus not every animal is represented. The nuclei of cuboidal epithelial cells lining the airway and at the bifurcation were counted. Brown nuclei positive for BrdU incorporation were then also counted and are reported as the percent BrdU positive epithelial cells at the terminal bronchial duct bifurcation.

Collagen Analysis.

Snap frozen right lung lobes were weighed out to 10 mg, homogenized and assayed for protein and soluble collagen. The Sircol soluble collagen kit (Biocolor, Carrickfergus, UK) was used to assay collagen content and the Pierce BCA protein assay (Thermo Scientific, Waltham, MA) was used to determine protein concentrations from each mouse lung. Area to perimeter ratio analysis was also conducted utilizing Masson’s Trichrome-stained mouse lungs by quantitatively measuring collagen surrounding the airways as described previously (Duke et al., 2017).

Inflammatory Quantification.

BALF was collected and 100 μL was cytospun onto slides. Cells were stained with the DiffQuik® stain set (Dade Behring Inc, Newark, DE). A differential cell count was performed on the BALF to determine the percentage of macrophages, eosinophils, neutrophils and lymphocytes. A total of 500 cells were counted per slide.

Cytokine Quantification.

Cytokines (total TGF-β1, osteopontin, and PDGF-BB) from BALF were measured by commercially available DuoSet enzyme linked immunosorbent assay (ELISA) kits (R & D Systems, Inc., Minneapolis, MN).

Transmission Electron Microscope (TEM).

As purchased tMWCNTs and rMWCNTs were imaged using a JEOL 2000FX scanning TEM and samples were prepared as described previously (Dandley et al., 2016). Lung tissue from mice exposed to either tMWCNTs or rMWCNTs was first fixed with formalin and embedded in paraffin then submitted to core TEM facilities for de-paraffinization and resin embedding.

Statistical Analysis.

Statistical analysis was done using GraphPad Prism software version 5.0 (GraphPad Software, Inc., San Diego, CA). A one-way ANOVA with a Tukey post-hoc test was performed to determine statistical differences between treatments and genotypes.

RESULTS

Survival.

All mice survived to the end of the study with the exception of three (Supplemental Figure 1). Two male mice in the $p53^{+/-}$ group treated with rMWCNT died early from unknown causes and one female mouse in the $p53^{+/-}$ group treated with tMWCNT was euthanized due to lymphoma formation.

MWCNTs in the lung tissue of mice 11 months post-initial exposure.

Transmission electron microscopy (TEM) of the bulk nanomaterials used in this study showed the contrasting geometric shapes between ‘tangled’ tMWCNTs and ‘rod-like’ rMWCNTs (Fig 1A, D). Singlet and agglomerated nanotube structures were present within pulmonary alveolar macrophages 11 months post-initial exposure to either t- or r-MWCNTs (Fig 1B-C, E-F). tMWCNTs were present intracellularly and within close proximity to the Golgi apparatus and the nuclear membrane, but not within the nucleus. rMWCNTs were also present intracellularly 11 months post-initial exposure and were found in singlet and in condensed aggregates. Light microscopy of lung sections from mice showed aggregates and singlets of tMWCNTs or rMWCNTs within alveolar macrophages (Fig 2A). Of note, the rMWCNTs, but not the tMWCNTs, protrude from macrophages indicating frustrated phagocytosis (Fig. 2A). In addition, crystalline bodies in the cytosol of alveolar macrophages were observed in the lungs of either $p53^{+/+}$ or $p53^{+/-}$ mice exposed to tMWCNTs (Fig. 2B arrows in tMWCNT panels). No crystalline bodies were observed in mouse lungs exposed to rMWCNTs.

Inflammatory cells and cytokines in BALF.

Macrophages dominated the immune cells in the bronchoalveolar lavage fluid (BALF) from mouse lungs from both genotypes and treatment groups. Though there was a slight increase

in neutrophil cell counts from the lungs of $p53^{+/+}$ mice with rMWCNT exposure, this increase was not significant (data not shown). Analysis of the cellular makeup of the BALF revealed that control, tMWCNT- or rMWCNT-exposed mice contained similar total cell counts (data not shown). Differential cell counts conducted on the cytospins of the BALF revealed predominantly macrophage-populated lungs with a slight, but not significant, increase in lymphocytes and neutrophils in lungs treated with rMWCNTs (data not shown). Cytokine levels of osteopontin (OPN), TGF-β1, and PDGF-BB in the BALF were not significantly increased by either MWCNT type or different between $p53^{+/+}$ and $p53^{+/-}$ mice at the chronic endpoint evaluated in this study (data not shown).

Granuloma formation in the lungs of $p53^{+/+}$ and $p53^{+/-}$ mice chronically exposed to tMWCNTs or rMWCNTs.

Mice exposed to tMWCNTs had multiple small granulomas mostly confined to the distal terminal bronchioles and alveolar ducts in the centriacinar region near the alveolar-bronchiolar junctions (Fig. 3A). There was a trend towards larger granuloma number and total granuloma area in t- or rMWCNT-exposed $p53^{+/-}$ mice compared to $p53^{+/+}$ mice, although this difference was not statistically significant (Fig. 3B, C). The macrophages containing t- or r- MWCNTs were enlarged with vacuolated cytoplasm, though the compacted agglomerates of tMWCNTs frequently obscured the macrophages. There were occasional multinucleated giant macrophages in the lungs of both $p53^{+/+}$ and $p53^{+/-}$ mice treated with either tMWCNTs or rMWCNTs. The locations of the granulomas associated with rMWCNTs were similar to the location of the granulomas seen with tMWCNT-exposed animals. The granulomas associated with rMWCNTs were qualitatively larger with greater cellularity compared to tMWCNTs, these granulomas contained numerous macrophages and often surrounded by lymphocytes (Fig. 3A). Rarely, there were rMWCNT-laden macrophages within the airway wall surrounded by increased numbers of fibroblasts. Foci of iBALT were observed near bronchioles with adjacent granulomas in the lungs of both $p53^{+/+}$ and $p53^{+/-}$ mice exposed to rMWCNTs but not tMWCNTs (Fig. 3D). Of note, there were significantly more granulomas adjacent to lymphoid tissue in the rMWCNT-exposed mouse lungs compared to the tMWCNT-exposed mouse lungs, and there was no notable difference between genotypes (Fig 3D).

Effect of p53 deficiency and MWCNT treatment on lymphoid tissue formation.

Bronchus-associated lymphoid tissue (BALT) is a tertiary lymphoid structure composed of lymphocytes (i.e. T and B cells) mainly along bifurcations of the upper airways and rarely forms in healthy human or mouse lungs. Inducible BALT (iBALT) can be induced during chronic inflammation, infection or other disease states (Sminia et al 1989; Foo and Phipps 2010). Both iBALT and non-bronchus-associated ectopic lymphoid tissue (ELT) structures were observed in mice from this study (Fig. 4C-D). The total number of lymphoid aggregates (iBALT and ELT) in tMWCNT-exposed mice was similar to that seen in the control animals, although there was a trend for increased numbers of lymphoid aggregates in $p53^{+/-}$ mice compared to $p53^{+/+}$ (Fig. 4A). The number of lymphoid aggregates significantly increased following rMWCNT, but induction of lymphoid aggregates by rMWCNTs was not different between $p53^{+/+}$ and $p53^{+/-}$ genotypes (Fig 4A). The percent of the lung occupied by lymphoid tissue, as measured by semi-quantitative morphometry, was significantly

greater in control $p53^{+/-}$ mice compared to control $p53^{+/+}$ mice, but was not further increased by tMWCNT or rMWCNT treatment (Fig. 4B). Taken together, these data suggest that while rMWCNTs increased the number of lymphoid aggregates, the area of lung occupied by these lymphoid structures was greater in $p53^{+/-}$ mouse lungs primarily due to constitutive iBALT in the absence of MWCNT exposure (Fig 4 E-F). iBALT lesions contained proliferating cells as observed with BrdU IHC staining, yet proliferation was similar in $p53^{+/+}$ and $p53^{+/-}$ mouse lungs regardless of MWCNT treatment (data not shown). Overexpression of cytokines like IL-6 are associated with inducing iBALT [47], yet we did not observe increased levels of IL-6 mRNA from treated mouse lung samples, nor did we detect increased transcription of chemokines CCL2, CXCL10 or CXCL9 at this time point (data not shown).

Structural organization of inducible tertiary lymphoid tissue.

To further characterize the lymphoid aggregates and granulomas, IHC stains for T cells (CD3+) and B cells (CD45R+/B220) were applied to serial lung sections. The cellular make-up of the inducible lymphoid tissues (iBALT and ELT) was classically ordered with a centrally-aggregated CD45R+ B cell population surrounded by more loosely distributed CD3+ T cells (Fig. 5). Despite non-specific staining of macrophage cytoplasm for CD3, close examination of the cellular morphology revealed that T and B cells were common in the periphery of both the r- and t-MWCNT-induced granulomas (data not shown). Prior studies of MWCNT exposure have shown increased T cell and macrophage staining around granulomas as well (Huizar et al., 2011; Huizar et al., 2013).

rMWCNT exposure resulted in increased DNA synthesis in cells within granulomas.

Lung tissue stained with BrdU was analyzed for brown-staining nuclei within granulomas that indicated proliferation (Fig. 6A). Each granuloma counted was validated by the presence of MWCNTs as described in the methods section. About 25% of the $p53^{+/+}$ and 15% of the $p53^{+/-}$ granulomas resulting from rMWCNT-exposure included BrdU positive cells compared to only 5% of either $p53^{+/+}$ or $p53^{+/-}$ tMWCNT-resulting lung granulomas (Fig. 6B).

Bronchiolar epithelial hyperplasia induced by MWCNT exposure.

Bronchiolar epithelial hyperplastic lesions were observed in the lungs of both $p53^{+/+}$ and $p53^{+/-}$ mice exposed to rMWCNTs, but were rarely observed in tMWCNT-exposed mouse lungs (Fig. 7A). Hyperplasia was measured by quantifying BrdU-positive bronchiolar epithelial cells. Quantification of BrdU-positive epithelial cells along the first bronchoalveolar duct bifurcation revealed increased proliferation in rMWCNT-exposed $p53^{+/+}$ and $p53^{+/-}$ mouse airway epithelial cells compared to control or tMWCNT treatment groups (Fig 7B). There were also occasional aggregates of plasma cells near airways of rMWCNT-exposed mice, which were not seen in the control or tMWCNT-exposed mouse lungs. In the animals exposed to rMWCNTs, there was a markedly increased incidence of bronchiolar epithelial hyperplasia at terminal bronchioles and a few instances of alveolar hyperplasia. Airway epithelial hyperplasia coupled with papillary hyperplasia (projection of epithelial cells into the lumen of the airway with simple connective tissue core present), could mark the transition towards neoplasia (Renne et al., 2009). A papillary hyperplastic

lesion in a small airway was observed in CD45R- and CD3-stained serial sections from a $p53^{+/-}$ mouse exposed to rMWCNTs (Fig. 8). Epithelial hyperplasia was a feature of rMWCNT-exposed mouse lungs, although differences between genotypes were not identified. However, the only evidence of papillary hyperplasia was found in one $p53^{+/-}$ mouse exposed to rMWCNTs.

Pulmonary fibrosis after chronic exposure to tMWCNTs or rMWCNTs.

Regional fibrosis was evident in Trichrome-stained lung sections from mice exposed to MWCNTs, primarily located within granulomas (Fig. 9A). rMWCNTs induced larger collagen-laden granulomas compared to tMWCNTs in both $p53^{+/+}$ and $p53^{+/-}$ mice. To determine if significant collagen deposition occurred after exposure to tMWCNTs or rMWCNTs, a quantitative Sircol assay was used to measure total lung collagen. Also, a semi-quantitative morphometric (area to perimeter ratio) analysis was performed to measure airway fibrosis. There was no significant difference in airway fibrosis (area to perimeter ratio) based on quantitative morphometry performed using the airway to perimeter ratio method (data not shown). The Sircol assay showed no difference in total collagen content from the lungs of $p53^{+/+}$ versus $p53^{+/-}$ mice (Fig. 9B). Moreover, there was no difference between genotypes in the tMWCNT exposure group. While $p53^{+/-}$ mice had significantly greater lung collagen content compared to $p53^{+/+}$ mice in the rMWCNT treatment group, this was due to a reduction in total lung collagen content in $p53^{+/+}$ mice exposed to rMWCNT.

Pleural lesions.

No evidence of pleural inflammation or mesothelioma was found in either $p53^{+/+}$ or $p53^{+/-}$ mice after careful examination of 3 H&E-stained sections per lung (data not shown).

DISCUSSION

The aim of this study was to examine the inflammatory, fibrogenic and carcinogenic potential of two types of MWCNTs with differing geometry (tangled versus rod-like) in the lungs of transgenic mice deficient in one allele of tumor suppressor p53. Because rMWCNTs have been classified as a Group 2B possible human carcinogen (IARC 2017), we postulated that chronic exposure to these rod-like nanotubes would cause lung cancer or mesothelioma in $p53^{+/-}$ but not wild type $p53^{+/+}$ mice. No MWCNT related lung tumors or mesothelioma were observed in $p53^{+/-}$ mice, although rMWCNTs caused focal bronchiolar epithelial hyperplasia in $p53^{+/-}$ mouse lungs. We observed a significant difference in pulmonary fibrosis (total lung collagen content) between $p53^{+/+}$ and $p53^{+/-}$ mice exposed to rMWCNTs but not tMWCNTs. Moreover, rMWCNTs caused more robust granuloma formation compared to tMWCNTs and there was a trend towards larger granulomas in $p53^{+/-}$ mice. Interestingly, we observed that rMWCNTs, but not tMWCNTs, stimulated iBALT formation in $p53^{+/+}$ mice and iBALT was spontaneously generated in the lungs of $p53^{+/-}$ mice. Also, $p53^{+/-}$ mice exhibited significantly larger lung area obscured by lymphoid aggregates compared to $p53^{+/+}$ mice. Overall, our findings indicate that p53 plays a role in constitutive iBALT formation in the lungs of mice and regulates rMWCNT-induced granuloma size.

Our study revealed a role for p53 in regulating granuloma formation after exposure to MWCNTs. The observation of increased BrdU-positive cells in granulomas from $p53^{+/+}$ or $p53^{+/-}$ mice after chronic exposure to rMWCNT is indicative of continual injury and/or immune stimulation. We observed that T cells were integrated into the granulomas induced by rMWCNTs (Fig. 5) and this is indicative of previously described immune granulomas that are positive for CD205, a marker of antigen-presenting cells (Ohtani 2013). Our observation of T cell infiltration within foreign body granulomas containing MWCNTs and the proximity of iBALT or ELT to many of these granulomas, especially in $p53^{+/-}$ mice, suggest ongoing immune responses in the lung tissue of rMWCNT-exposed mice.

The development of tertiary lymphoid tissues (iBALT and ELT) appears to be due to a combination of p53 deficiency and rMWCNT exposure in the lung. These foci form in response to chronic inflammation, infection or other disease states (Foo and Phipps 2010; Aloisi et al., 2006). The early development of this tissue is driven by IL-1α, and IL-1-receptor deficient mice fail to develop iBALT following exposure to either aluminum salts, silica, or viruses (Kuroda et al., 2016; Neyt et al., 2016). IL-6 also appears to play a role in the development of lymphoid-like structures in the lung (Goya et al., 2003). Interestingly, silica-induced lymphoid neogenesis can result in the development of an induced autoimmune phenotype (Bates et al., 2015). The lymphoid neogenesis exhibited in our study contained cellular elements organized into *de novo* formations of a B cell follicle surrounded by T cells (Aloisi et al., 2006). Additionally, increased iBALT in the lung is observed in mice as they age, and is further exacerbated by particulates found in cigarette smoke (John-Schuster et al., 2015). Previous examination of pulmonary exposure to rMWCNTs found that exposure resulted in the dilation of pulmonary lymphatics after 56 days as measured by indirect immunofluorescence of podoplanin, a lymphatic endothelial marker (Porter et al., 2010). Prior studies have observed MWCNTs deposited into BALT and have shown that these lymphoid tissues are a slower clearance method compared the mucociliary escalator in a rat model (Aiso et al., 2010). To date, there is no current literature available on p53 regulation or involvement of inducible lymphoid tissue development; however, p53 has been implicated in the immune response during development. For example, the co-regulatory function of NFκB and p53 increases IL-6 in primary human monocytes and macrophages and induces neutrophil chemokines (Lowe et al., 2014). In addition, following pulmonary infection with gram negative bacteria, p53 null or inhibited mice were able to clear the infection more quickly compared to wild type mice (Madenspacher et al., 2013). This clearance was due to increased phagocytosis, degranulation and NOX-dependent oxidant generation by neutrophils, yet these mice also exhibited high mortality following infection and clearance due to aggravated lung injury. It is possible that the increased iBALT formations observed in $p53^{+/-}$ mice in the present study could result in an altered immune microenvironment that could favor tumor development.

We observed that alveolar macrophages contained tMWCNTs or rMWCNTs at the end of our chronic study. Murine alveolar macrophages are a very long-lived cell, with a life-span that may potentially be as long as the animal itself (Murphy et al., 2008). Therefore, it was not surprising to observe MWCNTs in macrophages at nearly a year after exposure; i.e., approximately half the life span of the animal. In our study, the observation of BrdU-positive macrophages in granulomatous formations resulting from rMWCNT- and not from

tMWCNT-exposure lends itself to suggest that chronic injury by rMWCNTs could signal macrophage replenishment. Alveolar macrophages generally have a low proliferative index under normal homeostatic conditions, although they can self-replenish their population when the need arises during or following injury (Hashimoto et al., 2013). Infiltrating monocytes are also a source of macrophage replenishment in the lung as these cells differentiate into mature alveolar macrophages. Interestingly, alveolar macrophages from the lungs of $p53^{+/+}$ or $p53^{+/-}$ mice exposed to tMWCNTs contained crystalline bodies, but these bodies were not observed in macrophages from mice exposed to rMWCNTs. A study by Køobler and colleagues evaluated the pulmonary toxicity of a short, tangled MWCNT and two longer, thicker MWCNTs (one of which was Mitsui-7) at 1, 3 and 28 days and found crystalline bodies, described as eosinophilic crystalline pneumonia, within the cytosol of alveolar macrophages from mice exposed to all types of MWCNTs studied, but primarily in mice exposed to longer thicker MWCNTs (Køobler et al., 2015). They also reported that carbon black nanoparticle exposure did not increase crystal incidence above that seen in control animals and suggested that increased development of crystals might be related to shape and dimensions of carbon-based particles. In the present study, we observed crystalline bodies in macrophages from mice exposed to tMWCNT but not rMWCNTs. However, we assessed only a single chronic time point, so it is possible that crystalline bodies, if similar to the crystal structures described by Køobler and colleagues, could have been formed in lungs of rMWCNT-exposed mice early on, but resolved by the 11-month time point.

A major issue that we sought to address in this study was to determine if $p53^{+/-}$ mice, a mouse model that is susceptible to tumor development, would develop mesothelioma after pulmonary exposure to MWCNTs. Previous studies of $p53^{+/-}$ mice injected intraperitoneally with asbestos or rMWCNTs demonstrated more rapid development of mesotheliomas resulting from MWCNT compared to asbestos (Takagi et al., 2008; Takagi et al., 2012). We did not observe mesothelioma or other exposure-related neoplasms 11 months following the initial dose delivered by oropharyngeal aspiration in either wild type or $p53^{+/-}$ mice. Mesothelioma has been observed in mice following direct pulmonary exposure to asbestos. For example, Bozelka *et al.* used Balb/C mice and long-term inhalation exposure to chrysotile asbestos (2 hrs/day for 75 days) and demonstrated >90% of the animals developed tumors at the visceral pleura after 12 to 18 months (Bozelka et al., 1983). However, 10% of control (air exposed) Balb/C mice in that study developed tumors, suggesting that Balb/C mice are susceptible to tumor formation compared to the C57BL/6 strain used in our study. In addition, DBA/2J mice are more susceptible than C57BL/6 mice to aflatoxin-induced carcinogenesis (Hunter 2012). Therefore, it is not surprising that mesothelioma was not observed in $p53^{+/-}$ mice on a C57BL/6 background after MWCNT exposure in the present study. Overall this may indicate that mice, even transgenic strains that are susceptible to tumor promotion, are poor models for assessing the carcinogenic potential of MWCNTs. A study by Chernova and colleagues elegantly demonstrated mesothelioma on the chest wall (parietal pleura) of C57BL/6 mice after direct intrapleural injection of long MWCNTs or long asbestos fibers (Chernova et al., 2017). However, intrapleural injection by-passes the pulmonary route of administration and allows for a high bolus dose of MWCNTs directly to the pleural cavity, whereas pulmonary exposure by inhalation or oropharyngeal aspiration likely result in a very low exposure of MWCNT in the pleural cavity via translocation

through the pleural lymphatic drainage (Ryman-Rasmussen et al., 2009a). Rats appear to be more susceptible than mice as intratracheal instillation of rod-like MWCNTs into the lungs of F344 rats has been shown to cause mesothelioma (Suzui et al., 2016), a finding not yet seen in any strain of mouse exposed by direct pulmonary exposure to MWCNTs. Lung cancer but not mesothelioma was induced by the inhalation exposure of MWCNTs in rats (Kasai et al., 2016). Therefore, the method of pulmonary exposure (inhalation vs instillation) may be an important determinant of mesothelioma. Another caveat of our study is that the sample size of approximately ten mice per group may be insufficient statistical power to determine a negative carcinogenic effect as recommended by IARC (IARC 2017). Despite the lack of lung or pleural tumors in the present study, we observed epithelial hyperplasia resulting from pulmonary exposure to rMWCNTs which agrees in part with previous studies that showed epithelial hyperplasia and adenocarcinoma in the lungs of MWCNT-exposed rodents (Sargent et al., 2014; Kasai et al., 2016).

The fibrogenic and carcinogenic potential of MWCNTs has been compared to asbestos, a class of naturally occurring mineral fibers represented by different types; some more rigid than others. For example, rMWCNTs or crocidolite, a rigid type of asbestos, both resulted in mesothelioma when injected intraperitoneally in C57BL/6 mice or Wistar rats and progression of mesothelioma in these animals was coupled with an accumulation of monocytic cells that suppressed polyclonal activation of lymphocytes 12 months following exposure (Huaux et al., 2015). The rMWCNTs used in that study were the same used in our current study. Therefore, rMWCNTs appear to behave similarly to rod-like crocidolite asbestos fibers. The rodent model is limited by a short life span (~2 years), and a latency period of over 15 years is common for asbestos-induced mesothelioma or fibrosis in humans (Frost 2013; Prazakova et al., 2013). Since our chronic study did not reveal mesothelioma, it may be possible that a longer time period might be required (between 12 and 24 months) for tumorigenesis after direct pulmonary exposure.

A variety of physicochemical characteristics likely play an important role in the inflammatory, fibrotic and genotoxic responses to MWCNTs. Our study emphasized differences in nanotube geometry (i.e., tangled versus rod-like shape) although the two MWCNTs that we compared also had differences in other physicochemical characteristics such as length, surface area, surface charge, and residual metal catalyst content (Fe versus Ni). Other work has addressed physicochemical characteristics as predictors of disease outcome. For example, Poulsen and colleagues investigated the pulmonary exposure of 10 commercial MWCNTs in female C57BL/6J mice by intratracheal instillation and identified specific surface area (BET), length and surface oxidation as predictors of pulmonary inflammation, whereas larger MWCNT diameter predicted genotoxicity in lung cells (Poulsen et al., 2016). Therefore, it is likely that multiple physicochemical features play a role in the pathological responses to MWCNTs. In addition, it is also possible that physicochemical characteristics such as shape, length and charge may influence agglomeration status and the number of nanotubes per unit mass. We dosed mice on a mass basis, but it is possible that this approach results in differences in the number of MWCNTs delivered to the lungs of mice.

CONCLUSIONS

Our findings show that genetic susceptibility (loss of one allele encoding the p53 tumor suppressor) plays a role in the immune response to MWCNT exposure in mice. A constitutively larger area of $CD45R^{+}/CD3^{+}$ lymphoid tissue was observed in the lungs of $p53^{+/-}$ mice compared to $p53^{+/+}$ mice and these mice had larger granulomas induced by either tMWCNTs or rMWCNTs as compared to $p53^{+/+}$ mice, with rMWCNTs causing the most prominent granuloma formation. While no lung or pleural tumors were observed in $p53^{+/-}$ mice after chronic MWCNT exposure, rMWCNTs caused greater epithelial cell hyperplasia in terminal bronchioles in both $p53^{+/-}$ and $p53^{+/+}$ mice. These findings indicate that both p53 deficiency and physicochemical features including nanotube geometry are factors in susceptibility to MWCNT-induced lymphoid infiltration and granuloma formation.

Supplementary Material

Refer to Web version on PubMed Central for supplementary material.

Acknowledgments

We are grateful for the help of Dr. Erinn Needham-Dandley for her expertise in TEM imaging of the as purchased MWCNTs.

Funding

This work was supported by NIEHS R01ES020897 (JCB, KSD, EAA, MDI, KAS, EAT, AJT), NIEHS Training Grant: T32 ES007046 (KSD, MDI), NIEHS P30 ES025128 (DAT), the NIEHS Intramural Program (MFC) and NIOSH (LMS, DWP, AFH).

LIST OF ABBREVIATIONS

BALF	Bronchoalveolar lavage fluid
iBALT	Inducible bronchus-associated lymphoid tissue
BrdU	BromodeoxyuridineCD45R - B cell marker
CD3	T cell marker
CNT	Carbon nanotube
CCL2	Chemokine (C-C motic) ligand 2
CXCL10	C-X-C motif chemokine 10
CXCL9	C-X-C motif chemokine 9
DPBS	Dulbecco’s phosphate-buffered saline
ELISA	Enzyme linked immunosorbent assay
ELT	Ectopic lymphoid tissue
IHC	Immunohistochemistry

IL	Interleukin
MCA	Methylcholanthrene
MWCNT	Multi-walled carbon nanotube
tMWCNT	Tangled MWCNT
rMWCNT	Rod-like MWCNT
NF-κB	Nuclear factor kappa-light-chain-enhancer of activated B cells
OPN	Osteopontin
PDGF	Platelet derived growth factor
$p53^{+/-}$	Heterozygous for the p53 allele
OPA	Oropharyngeal aspiration
TGF-β1	Transforming growth factor β1
TEM	transmission electron microscope

REFERENCES

Agarwal M, Agarwal A, Taylor W, Stark G. p53 controls both the G2/M and the G1 cell cycle checkpoints and mediates reversible growth arrest in human fibroblasts. PNAS. 1995;92:8493–7. [PubMed: 7667317]

Aiso S, Yamazaki K, Umeda Y, Asakura M, Kasai T, Takaya M, et al. Pulmonary Toxicity of Intratracheally Instilled Multiwall Carbon Nanotubes in Male Fischer 344 Rats. Ind Health. 2010;48:783–95. [PubMed: 20616469]

Aloisi F, Pujol-Borrell R. Lymphoid neogenesis in chronic inflammatory diseases. Nat Rev Immunol. 2006;6:205–17. [PubMed: 16498451]

Barrett JC, Lamb PW, Wiseman RW. Multiple mechanisms for the carcinogenic effects of asbestos and other mineral fibers. Environ Health Perspect. 1989;81:81–9. [PubMed: 2667990]

Bates MA, Brandenberger C, Langohr I. Silica Triggers Inflammation and Ectopic Lymphoid Neogenesis in the Lungs in Parallel with Accelerated Onset of Systemic Autoimmunity and Glomerulonephritis in the Lupus-Prone NZBWF1 Mouse. PLoS One. 2015;10(5):e0125481.2015;:1–25. [PubMed: 25978333]

Bozelka BE, Sestini P, Gaumer HR, Hammad Y, Heather CJ, Salvaggio JE. A murine model of asbestosis. Am J Pathol. 1983;112:326–37. [PubMed: 6311019]

Chernova T, Murphy FA, Galavotti S, Sun XM, Powley IR, Grosso S, Schinwald A, Zacarias-Cabeza J, Dudek KM, Dinsdale D, Le Quesne J, Bennett J, Nakas A, Greaves P, Poland CA, Donaldson K, Bushell M, Willis AE, MacFarlane M Long-fiber carbon nanotubes replicate asbestos-induced mesothelioma with disruption of the tumor suppressor gene Cdkn2a (Ink4a/Arf). Curr Biol. 2017; 27(21):3302–3314.e6. [PubMed: 29112861]

Dai C, Gu W. P53 post-translational modification: Deregulated in tumorigenesis. Trends Mol Med. 2010;16:528–36. [PubMed: 20932800]

Dandley EC, Taylor AJ, Duke KS, Ihrie MD, Shipkowski KA, Parsons GN, et al. Atomic layer deposition coating of carbon nanotubes with zinc oxide causes acute phase immune responses in human monocytes in vitro and in mice after pulmonary exposure. Part Fibre Toxicol. 2016;13:29. [PubMed: 27278808]

Donaldson K, Aitken R, Tran L, Stone V, Duffin R, Forrest G, and Alexander A (2006). Carbon nanotubes: A review of their properties in relation to pulmonary toxicology and workplace safety. Toxicol. Sci, 92, 5–22. [PubMed: 16484287]

Dong J, Porter DW, Batteli LA, Wolfarth MG, Richardson DL, Ma Q. Pathologic and molecular profiling of rapid onset fibrosis and inflammation induced by multi walled carbon nanotubes. Arch Toxicol. 2014;89:621–33. [PubMed: 25510677]

Duke KS and Bonner JC (2018). Mechanisms of carbon nanotube-induced pulmonary fibrosis: a physicochemical characteristic perspective. Wiley Interdiscip. Rev. Nanomedicine Nanobiotechnology, 10, e1498. [PubMed: 28984415]

Duke KS, Taylor-Just AJ, Ihrie MD, Shipkowski KA, Thompson EA, Dandley EC, et al. STAT1-dependent and -independent pulmonary allergic and fibrogenic responses in mice after exposure to tangled versus rod-like multi-walled carbon nanotubes. Part Fibre Toxicol. 2017;14:26. [PubMed: 28716119]

Foo SY, Phipps S. Regulation of inducible BALT formation and contribution to immunity and pathology. Mucosal Immunol. 2010;3:537–44. [PubMed: 20811344]

Frost G The latency period of mesothelioma among a cohort of British asbestos workers (1978–2005). Br J Cancer. 2013;109:1965–73. [PubMed: 23989951]

Goya S, Matsuoka H, Mori M, Morishita H, Kida H, Kobashi Y, et al. Sustained interleukin-6 signalling leads to the development of lymphoid organ-like structures in the lung. J Pathol. 2003;200:82–7. [PubMed: 12692845]

Hashimoto D, Chow A, Noizat C, Teo P, Beasley MB, Leboeuf M, et al. Tissue-Resident Macrophages Self-Maintain Locally throughout Adult Life with Minimal Contribution from Circulating Monocytes. Immunity. 2013;38:792–804. [PubMed: 23601688]

Hilton GM, Taylor AJ, Hussain S, Dandley EC, Griffith EH, Garantziotis S, Parsons GN, Bonner JC, Bereman MS. Mapping differential cellular protein response of mouse alveolar epithelial cells to multi-walled carbon nanotubes as a function of atomic layer deposition coating. Nanotoxicology. 2017; 11(3):313–326. [PubMed: 28277982]

Hojo S, Fujita J, Yamadori I, Kamei T, Yoshinouchi T, Ohtsuki Y, et al. Heterogeneous point mutations of the p53 gene in pulmonary fibrosis. Eur Respir J. 1998;12:1404–8. [PubMed: 9877499]

Hubbs AF, Mercer RR, Benkovic SA, Harkema J, Sriram K, Schwegler-Berry D, et al. Nanotoxicology—A Pathologist's Perspective. Toxicol Pathol. 2011;39:301–24. [PubMed: 21422259]

Huaux F, d'Ursel de Bousies V, Parent M-A, Orsi M, Uwambayinema F, Devosse R, et al. Mesothelioma response to carbon nanotubes is associated with an early and selective accumulation of immunosuppressive monocytic cells. Part Fibre Toxicol. 2015;13:46.

Huizar I, Malur A, Patel J, Mcpeek M, Dobbs L, Wingard C, et al. The role of PPAR γ in carbon nanotube-elicited granulomatous lung inflammation. Respir Res. 2013;14:1. [PubMed: 23289668]

Huizar I, Malur A, Midgette YA, Kukoly C, Chen P, Ke PC, et al. Novel murine model of chronic granulomatous lung inflammation elicited by carbon nanotubes. Am J Respir Cell Mol Biol. 2011;45:858–66. [PubMed: 21398620]

Hunter KW. Mouse models of cancer: does the strain matter? Nat Rev Cancer. 2012: 19; 12(2):144–9. [PubMed: 22257951]

IARC (International Agency for Research on Cancer) Working Group on the Evaluation of Carcinogenic Risks to Humans. Some nanomaterials and some fibres. 2017.

John-Schuster G, Günter S, Hager K, Conlon TM, Eickelberg O, Yildirim AÖ. Inflammaging increases susceptibility to cigarette smoke-induced COPD. Oncotarget. 2015.

Kasai T, Umeda Y, Ohnishi M, Mine T, Kondo H, Takeuchi T. Lung carcinogenicity of inhaled multi-walled carbon nanotube in rats. Part Fibre Toxicol. 2016;1–19. [PubMed: 26746196]

Købler C, Poulsen SS, Saber AT, Jacobsen NR, Wallin H, Yauk CL, Halappanavar S, Vogel U, Qvortrup K, Mølhave K. Time-dependent subcellular distribution and effects of carbon nanotubes in lungs of mice. PLoS One. 2015; 10(1):e0116481. [PubMed: 25615613]

Kuick Research. Global Carbon Nanotubes Market and Patent Insight 2023. 2017.

Kuroda E, Ozasa K, Temizoz B, Ohata K, Koo CX, Kanuma T, et al. Inhaled Fine Particles Induce Alveolar Macrophage Death and Interleukin-1α Release to Promote Inducible Bronchus-Associated Lymphoid Tissue Formation. Immunity. 2016;45:1299–310. [PubMed: 28002730]

Lowe JM, Menendez D, Bushel PR, Shatz M, Kirk EL, Troester MA, et al. p53 and NF-κB coregulate proinflammatory gene responses in human macrophages. Cancer Res. 2014;74:2182–2192. [PubMed: 24737129]

Madenspacher JH, Azzam KM, Gowdy KM, Malcolm KC, Nick JA, Dixon D, et al. P53 Integrates Host Defense and Cell Fate During Bacterial Pneumonia. J Exp Med. 2013;210:891–904. [PubMed: 23630228]

Mercer RR, Scabilloni JF, Hubbs AF, Wang L, Battelli L a, McKinney W, et al. Extrapulmonary transport of MWCNT following inhalation exposure. Part Fibre Toxicol. 2013;10:13. [PubMed: 23587247]

Mercer RR, Hubbs AF, Scabilloni JF, Wang L, Battelli LA, Friend S, Castranova V, Porter DW. Pulmonary fibrotic response to aspiration of multi-walled carbon nanotubes. Part Fibre Toxicol. 2011; 8:21. [PubMed: 21781304]

Muller J, Huaux F, Moreau N, Misson P, Heilier JF, Delos M, et al. Respiratory toxicity of multi-wall carbon nanotubes. Toxicol Appl Pharmacol. 2005;207:221–31. [PubMed: 16129115]

Murphy F, Schinwald A, Poland C, Donaldson K. The mechanism of pleural inflammation by long carbon nanotubes: interaction of long fibres with macrophages stimulates them to amplify pro-inflammatory responses in mesothelial cells. Part Fibre Toxicol. 2012;9:8. [PubMed: 22472194]

Murphy J, Summer R, Wilson AA, Kotton DN, Fine A. The prolonged life-span of alveolar macrophages. Am J Respir Cell Mol Biol. 2008;38:380–5. [PubMed: 18192503]

Nagai H, Okazaki Y, Chew S, Misawa N, Yamashita Y, Akatsuka S, et al. Diameter and rigidity of multiwalled carbon nanotubes are critical factors in mesothelial injury and carcinogenesis. Proc Natl Acad Sci USA. 2011; 108(49):E1330–8. [PubMed: 22084097]

Neyt K, GeurtsvanKessel CH, Deswarte K, Hammad H, Lambrecht BN. Early IL-1 Signaling Promotes iBALT Induction after Influenza Virus Infection. Front Immunol. 2016;7:312. [PubMed: 27579026]

Ohtani H Granuloma cells in chronic inflammation express CD205 (DEC205) antigen and harbor proliferating T lymphocytes: similarity to antigen-presenting cells. Pathol Int. 2013;63:85–93. [PubMed: 23464965]

Poland C, Duffin R, Kinloch I, Maynard A, Wallace W a H, Seaton A, et al. Carbon nanotubes introduced into the abdominal cavity of mice show asbestos-like pathogenicity in a pilot study. Nat Nanotechnol. 2008;3:423–8. [PubMed: 18654567]

Porter DW, Hubbs AF, Mercer RR, Wu N, Wolfarth MG, Sriram K, et al. Mouse pulmonary dose- and time course-responses induced by exposure to multi-walled carbon nanotubes. Toxicology. 2010;269:136–47. [PubMed: 19857541]

Poulsen SS, Jackson P, Kling K, Knudsen KB, Skaug V, Kyjovska ZO, Thomsen BL, Clausen PA, Atluri R, Berthing T, Bengtson S, Wolff H, Jensen KA, Wallin H, Vogel U. Multi-walled carbon physicochemical properties predict pulmonary inflammation and genotoxicity. Nanotoxicology. 2016; 10(9):1263–75. [PubMed: 27323647]

Prazakova S, Thomas PS, Sandrini A, Yates DH. Asbestos and the lung in the 21st century: an update. Clin Respir J. 2014;8:1–10. [PubMed: 23711077]

Preibisch S, Saalfeld S, Tomancak P. Globally optimal stitching of tiled 3D microscopic image acquisitions. Bioinformatics. 2009;25:1463–5. [PubMed: 19346324]

Renne R, Brix A, Harkema J, Herbert R, Kittel B, Lewis D, et al. Proliferative and Nonproliferative Lesions of the Rat and Mouse Respiratory Tract. Toxicol Pathol. 2009;37 7_suppl:5S–73S. [PubMed: 20032296]

Rittinghausen S, Hackbarth A, Creutzenberg O, Ernst H, Heinrich U, Leonhardt A, et al. The carcinogenic effect of various multi-walled carbon nanotubes (MWCNTs) after intraperitoneal injection in rats. Part Fibre Toxicol. 2014;11:59. [PubMed: 25410479]

Ryman-rasmussen JP, Cesta MF, Brody AR, Shipley- JK, Everitt J, Tewksbury EW, et al. Inhaled Carbon Nanotubes Reach the Sub-Pleural Tissue in Mice. Nat Nanotechnol. 2009a;4:747–51. [PubMed: 19893520]

Ryman-Rasmussen JP, Tewksbury EW, Moss OR, Cesta MF, Wong BA, Bonner JC. Inhaled multiwalled carbon nanotubes potentiate airway fibrosis in murine allergic asthma. Am J Respir Cell Mol Biol. 2009b;40:349–58. [PubMed: 18787175]

Sakamoto Y, Nakae D, Fukumori N, Tayama K, Maekawa A, Imai K, et al. Induction of mesothelioma by a single intrascrotal administration of multi-wall carbon nanotube in intact male Fischer 344 rats. J Toxicol Sci. 2009;34:65–76. [PubMed: 19182436]

Sargent LM, Porter DW, Staska LM, Hubbs AF, Lowry DT, Battelli L, et al. Promotion of lung adenocarcinoma following inhalation exposure to multi-walled carbon nanotubes. Part Fibre Toxicol. 2014;11:3. [PubMed: 24405760]

Schneider CA, Rasband WS, Eliceiri KW. NIH Image to ImageJ: 25 years of image analysis. Nat Methods. 2012;9:671–5. [PubMed: 22930834]

Siegrist KJ, Reynolds SH, Kashon ML, Lowry DT, Dong C, Hubbs AF, et al. Genotoxicity of multi-walled carbon nanotubes at occupationally relevant doses. Part Fibre Toxicol. 2014;11. [PubMed: 24529161]

Sminia T, van der Brugge-Gamelkoorn GJ, Jeurissen SH. Structure and function of bronchus-associated lymphoid tissue (BALT). Crit Rev Immunol. 1989;9:119–50. [PubMed: 2663024]

Suzui M, Futakuchi M, Fukamachi K, Numano T, Abdelgied M, Takahashi S, et al. Multiwalled carbon nanotubes intratracheally instilled into the rat lung induce development of pleural malignant mesothelioma and lung tumors. Cancer Sci. 2016;107:924–35. [PubMed: 27098557]

Takagi A, Hirose A, Nishimura T, Fukumori N, Ogata A, Ohashi N, et al. Induction of mesothelioma in p53+/− mouse by intraperitoneal application of multi-wall carbon nanotube. J Toxicol Sci. 2008;33:105–16. [PubMed: 18303189]

Takagi A, Hirose A, Futakuchi M, Tsuda H, Kanno J. Dose-dependent mesothelioma induction by intraperitoneal administration of multi-wall carbon nanotubes in p53 heterozygous mice. Cancer Sci. 2012;103:1440–4. [PubMed: 22537085]

Takahashi T, Munakata M, Ohtsuka Y, Nisihara H, Nasuhara Y, Kamachi-Satoh A, et al. Expression and alteration of ras and p53 proteins in patients with lung carcinoma accompanied by idiopathic pulmonary fibrosis. Cancer. 2002;95:624–33. [PubMed: 12209756]

Vancheri C, Failla M, Crimi N, Raghu G. Idiopathic pulmonary fibrosis: A disease with similarities and links to cancer biology. Eur Respir J. 2010;35:496–504. [PubMed: 20190329]

Wang Y, Zhang Z, Lubet R a, You MA mouse model for tumor progression of lung cancer in ras and p53 transgenic mice. Oncogene. 2006;25:1277–80. [PubMed: 16247444]

Wang Y, Suh YA, Fuller MY, Jackson JG, Xiong S, Terzian T, et al. Restoring expression of wild-type p53 suppresses tumor growth but does not cause tumor regression in mice with a p53 missense mutation. J Clin Invest. 2011b;121:893–904. [PubMed: 21285512]

Xu B, Guenther JF, Pociask D a., Wang Y, Kolls JK, You Z, et al. Promotion of lung tumor growth by interleukin-17. AJP Lung Cell Mol Physiol. 2014;307:L497–508.

Xu J, Futakuchi M, Shimizu H, Alexander DB, Yanagihara K, Fukamachi K, et al. Multi-walled carbon nanotubes translocate into the pleural cavity and induce visceral mesothelial proliferation in rats. Cancer Sci. 2012;103:2045–50. [PubMed: 22938569]

Xu J, Alexander DB, Futakuchi M, Numano T, Fukamachi K, Suzui M, et al. Size- and shape-dependent pleural translocation, deposition, fibrogenesis, and mesothelial proliferation by multiwalled carbon nanotubes. Cancer Sci. 2014;105:763–9. [PubMed: 24815191]

Zilfou JT, Lowe SW. Tumor suppressive functions of p53. Cold Spring Harb Perspect Biol. 2009;1:a001883. [PubMed: 20066118]

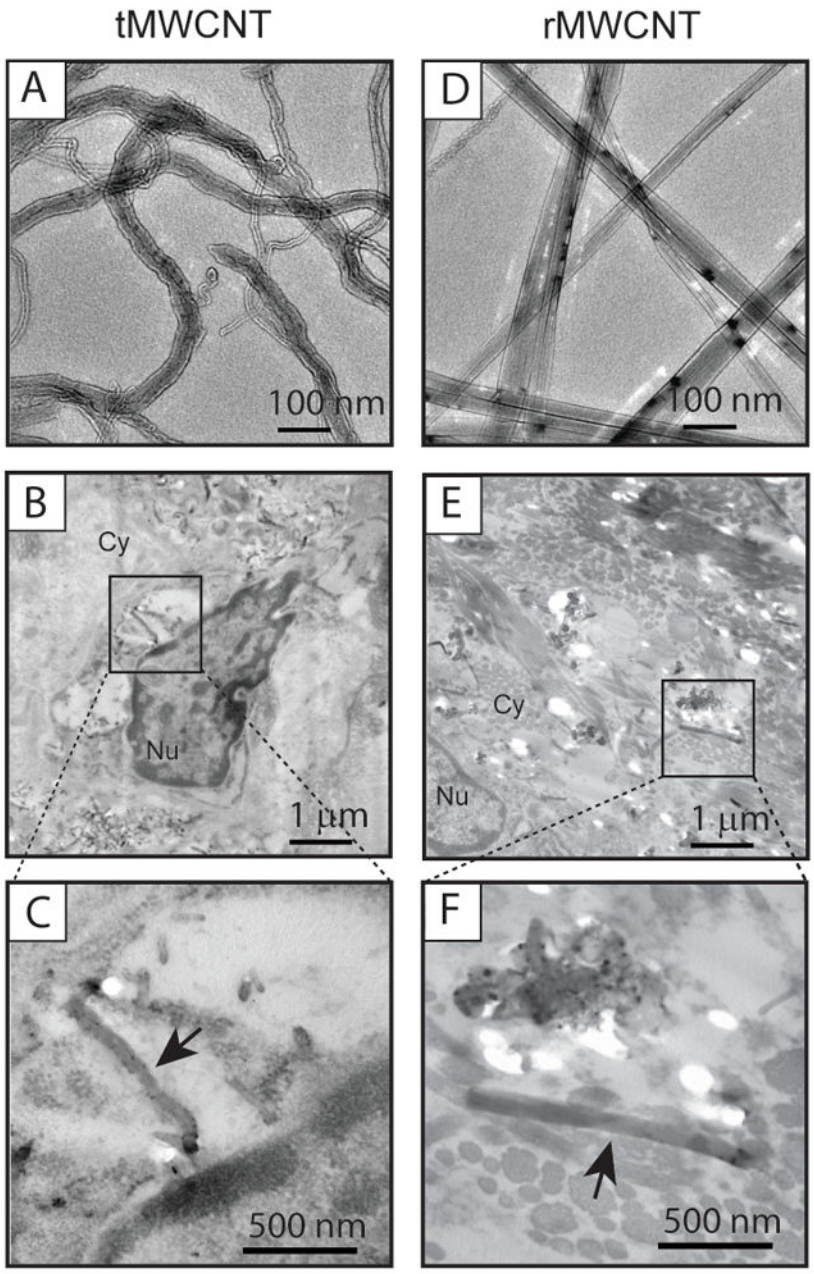

Figure 1.

TEM images of nanomaterials used in the study A) tMWCNTs and D) rMWCNTs. B) TEM image of tMWCNTs in lung granuloma from a $p53^{+/-}$ mouse at 11 months post-exposure. Cy indicates cytoplasm, and Nu indicates the nucleus. C) Inset showing a representative tMWCNT (arrow) near the nuclear membrane of a phagocytic cell. E) TEM image of rMWCNTs in granulomatous connective tissue from a $p53^{+/-}$ mouse at the end of the 11-month study period. F) Inset showing a representative rMWCNT (arrow).

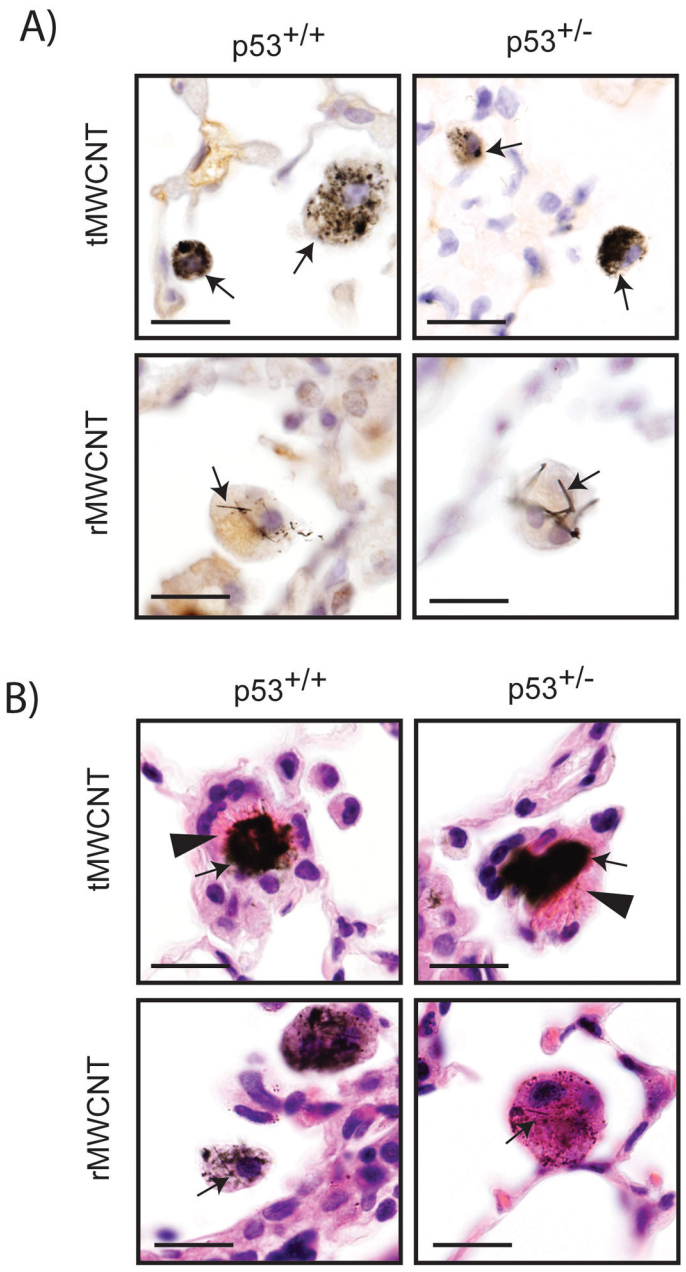

Figure 2.

Pulmonary alveolar macrophages containing tMWCNTs or rMWCNTs in the lungs of mice at the end of the 11-month study period. A) Hematoxylin-stained mouse lung tissue from both wild type and $p53^{+/-}$ with arrows indicating the enclosed foreign material within the alveolar macrophages in the lungs (scale bar equals 20 μm). B) Hematoxylin & Eosin-stained (H&E) lung tissue from wild type and $p53^{+/-}$ mice with arrows indicating macrophages containing tMWCNTs or rMWCNTs. Arrowheads indicate crystalline bodies within the cytosol of alveolar macrophages (scale bars equal 20 μm).

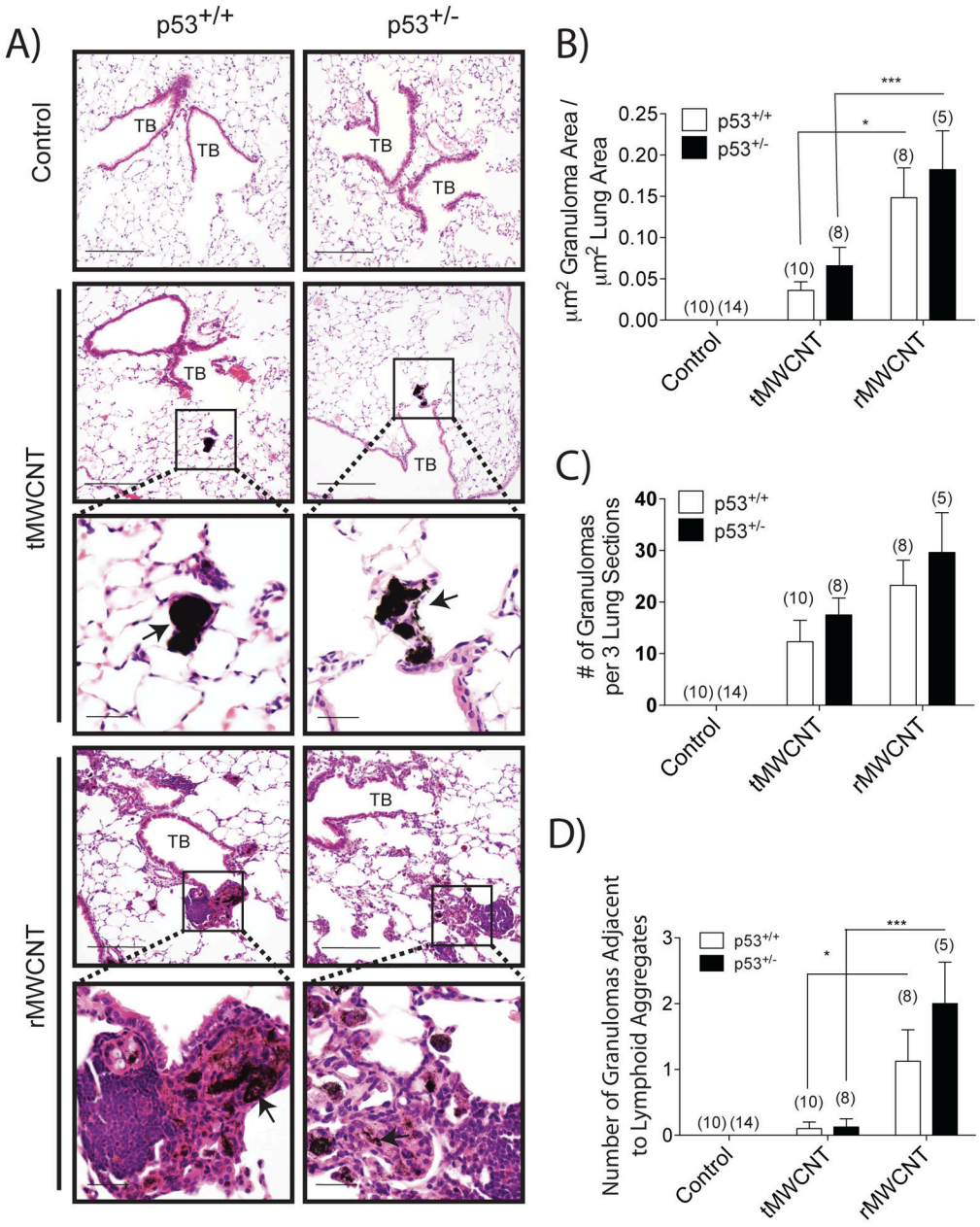

Figure 3.

rMWCNT exposure results in significantly larger lung granuloma area and a higher association with lymphoid tissue compared to tMWCNT, with a trend of larger formations in the lungs of $p53^{+/-}$ mice. A) H&E stained lung sections from wild type and $p53^{+/-}$ mouse lungs exposed to t- or r- MWCNTs near the terminal bronchioles (TB) of the lungs. Insets depict matured granuloma formations as indicated by arrows. (scale bar equal 200 μm, inset scale bars equal 50 μm). B) Average area of lung occupied by granuloma measured by quantitative morphometry (***$p<0.001$, *$p<0.05$ between tMWCNTs and rMWCNTs). C) Average number of granulomas per three lung sections per mouse. D) Average number of granulomas directly adjacent to lymphoid tissue per three lung sections per mouse. Number

in parentheses above graph bar indicates number of animals per group. (***p<0.001, *p<0.05 between tMWCNTs and rMWCNTs).

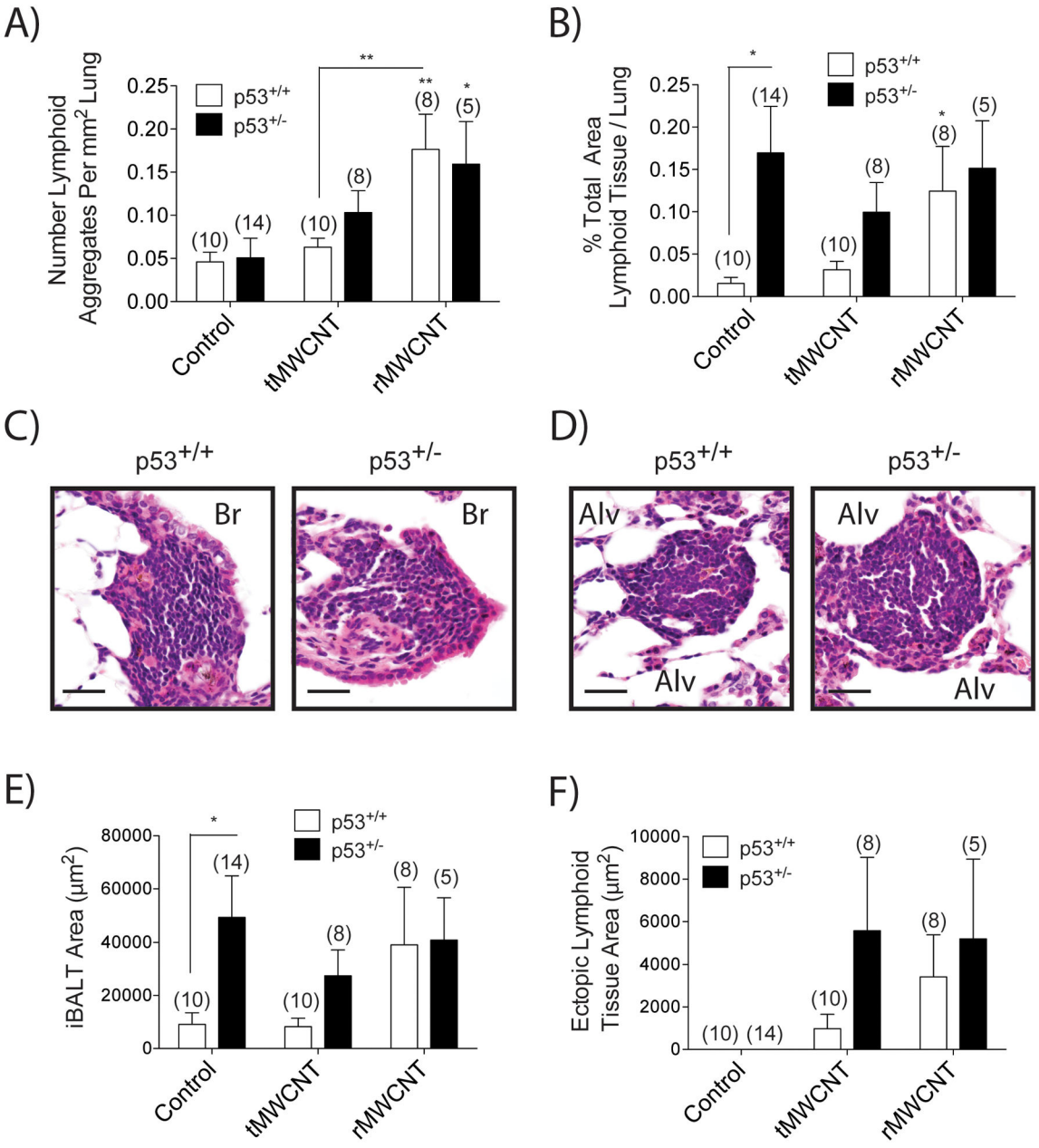

Figure 4.

Formation of inducible lymphoid tissue in response to tMWCNT or rMWCNT exposure. A) Average number of lymphoid aggregates as a function of square mm lung area (**p<0.01 between tMWCNT and rMWCNT, **p<0.01, *p<0.05 compared to control). B) Average percent of lung area occupied by lymphoid tissue measured by quantitative morphometry (*p<0.05 between genotypes, *p<0.05 compared to control). C) Inducible bronchus associated lymphoid tissue (iBALT) along the bronchial (Br) airway and D) ectopic lymphoid tissue (ELT) and surrounding alveolar (Alv) space of the lung of a wild type and $p53^{+/-}$ mouse lung exposed to rMWCNTs (scale bars equal 50 µm). Lymphoid tissue area

broken up into average area of E) iBALT and F) ELT (*p<0.05 between genotypes). Number in parentheses above graph bar indicates number of animals per group.

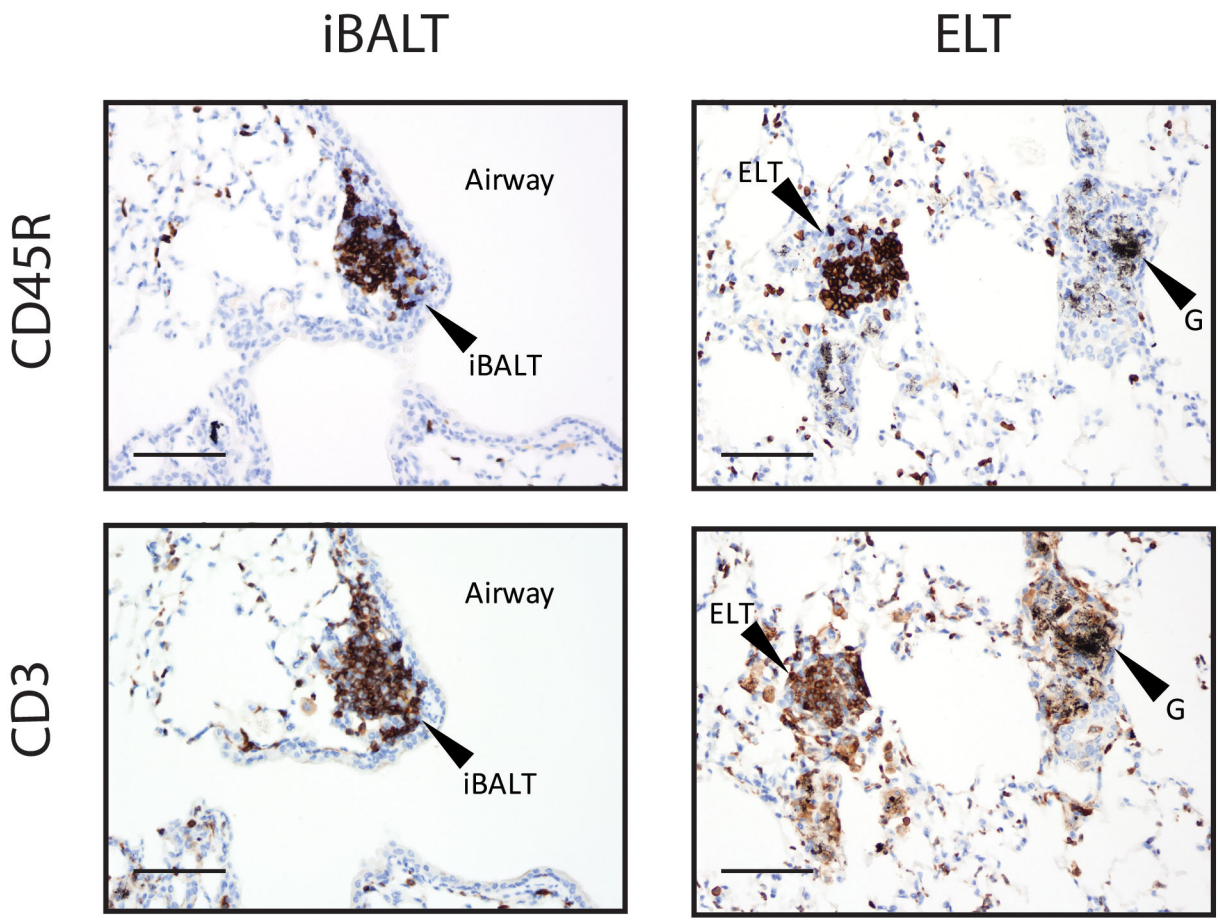

Figure 5.

Structure of pulmonary inducible lymphoid tissue. Lung tissue from $p53^{+/-}$ mice exposed to rMWCNTs for 11 months was immunohistochemically stained for the T cell marker CD3 and the B cell marker CD45R (B220) depicting a B cell germinal center with peripheral T cells in both the iBALT and ELT formations. For reference a granuloma (G) is indicated to show negative staining of cellular aggregates (scale bars equal 100 μm).

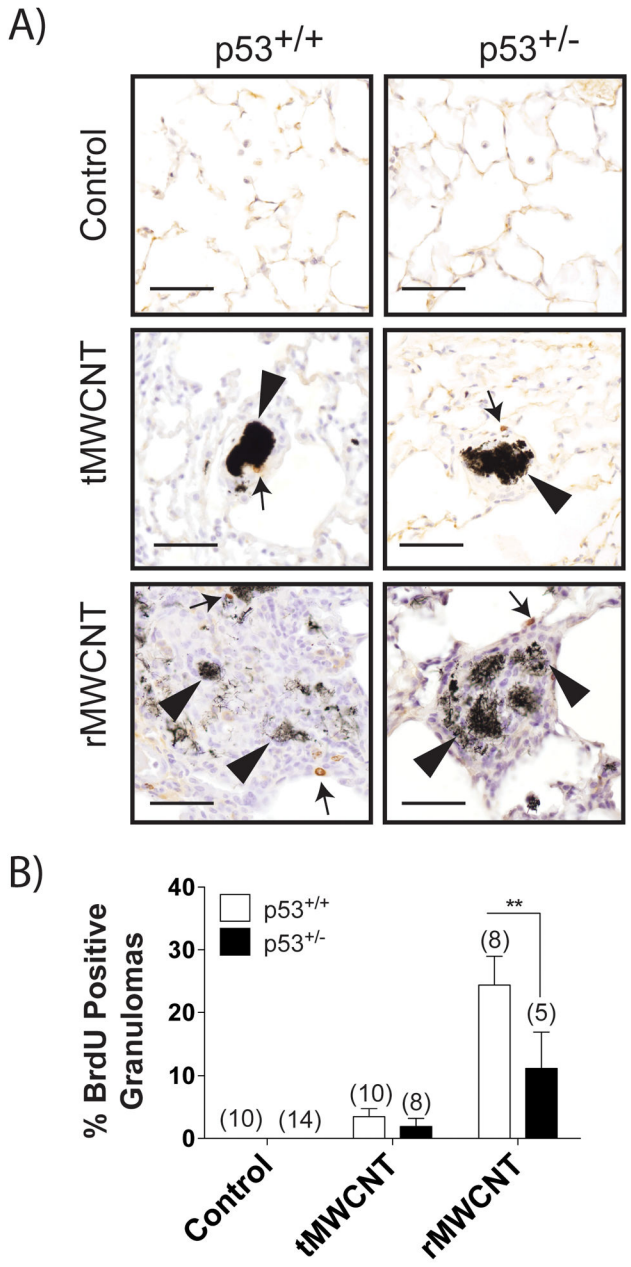

Figure 6.

BrdU IHC staining of mouse lungs from control and MWCNT-resultant granulomas show increased proliferation with rMWCNT exposure. A) Tissue from wild type and $p53^{+/-}$ mouse lungs exposed to t- or r- MWCNTs for 11 months was stained with BrdU where a dark brown stain indicates DNA synthesis and is also indicated by arrows. Arrowheads indicate the nanomaterial within the granuloma (scale bars equal 50 μm). B) Average number of granulomas with BrdU positively stained nuclei (**$p<0.01$ between genotypes). Number in parentheses above graph bar indicates number of animals per group.

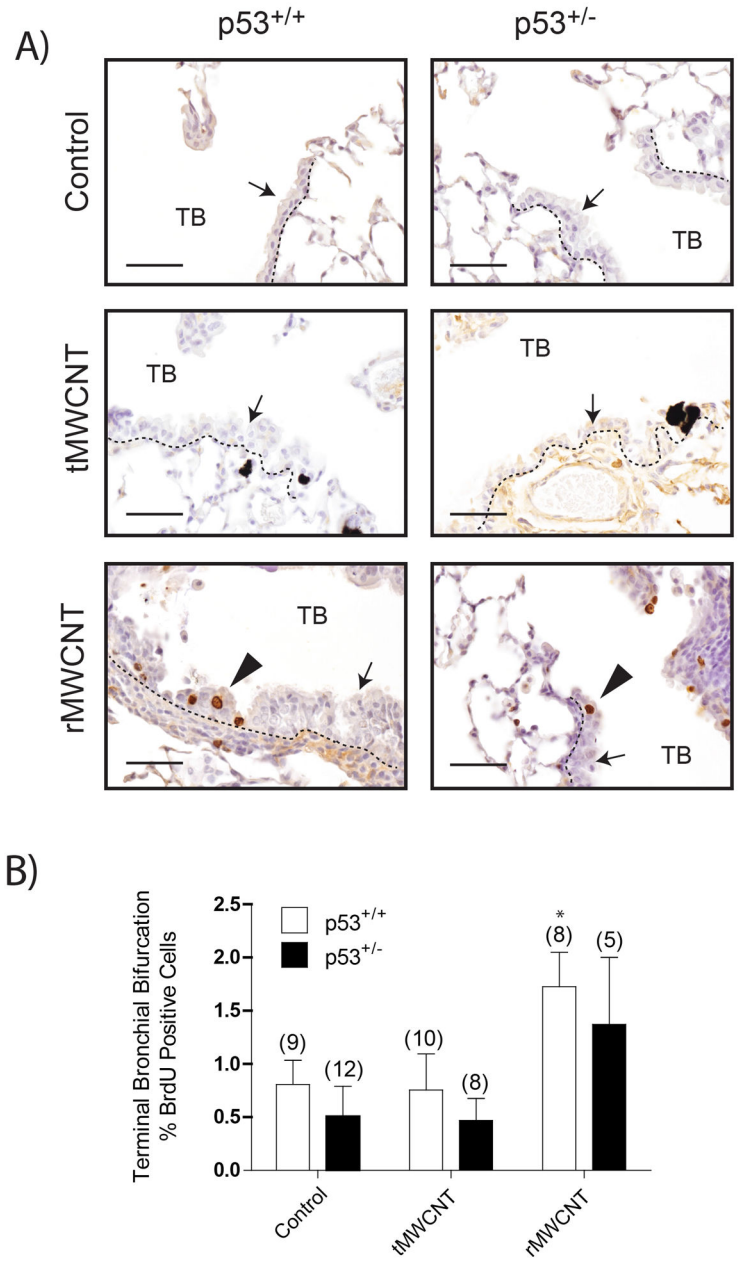

Figure 7.

Bronchiolar hyperplasia. A) BrdU stained lung sections from control, tMWCNT and rMWCNT wild type and $p53^{+/-}$ mice were imaged to show the bronchial epithelium near a terminal bronchiole (TB) as indicated by arrows. Arrowheads indicate BrdU positive epithelial cells in the hyperplastic epithelium (scale bars equal 50 μm). B) Quantitation of BrdU positive epithelial cells at the terminal bronchial bifurcation reported as %BrdU positive cells with standard error. Numbers in parenthesis indicate the number of animals analyzed per group. (*$p<0.05$ compared to control)

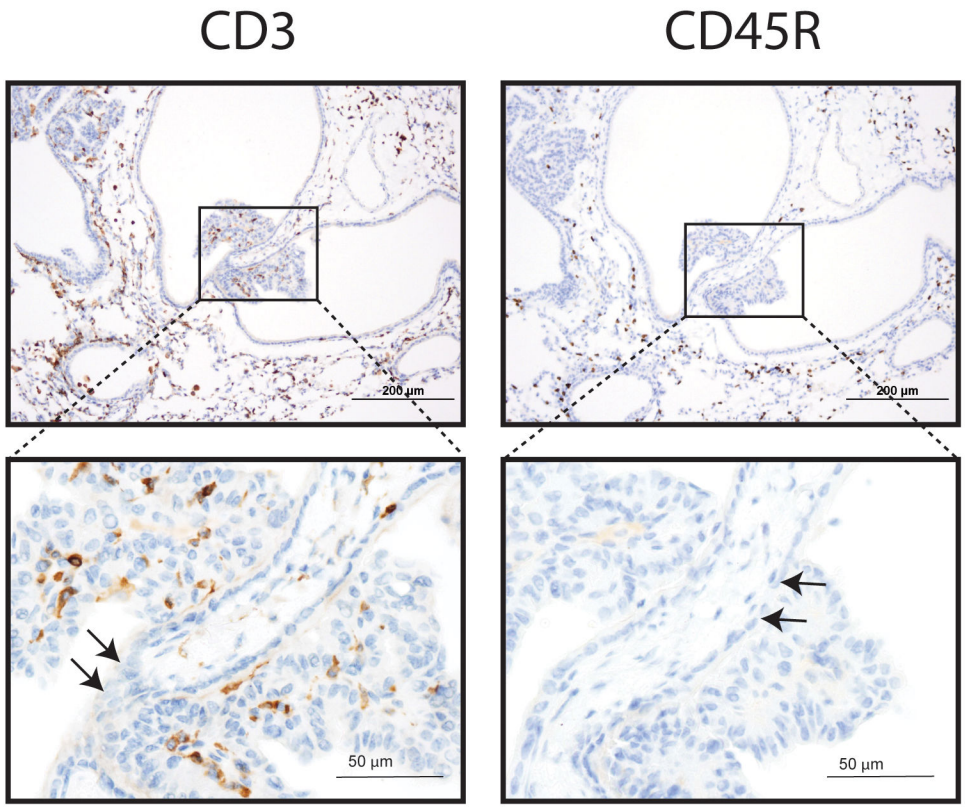

Figure 8.

Papillary hyperplasia of the bronchiolar epithelium at alveolar duct bifurcation. Serial sections of papillary hyperplasia at the terminal bronchus in a $p53^{+/-}$ mouse 11 months post-initial exposure to rMWCNTs. This rare pathology was captured in the IHC T cell marker CD3 and B cell marker CD45R sections. Arrows indicate location of papillary attachment to the bronchiole wall (scale bars equal 200 µm, inset scale bars equal 50 µm).

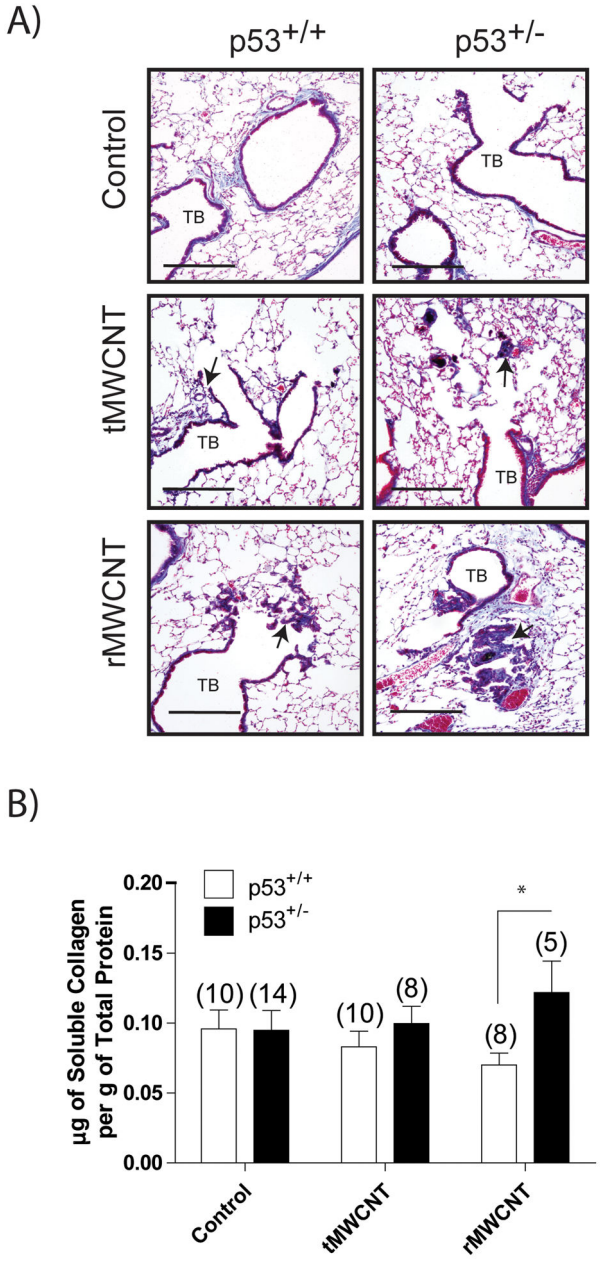

Figure 9.

Collagen deposition 11 months following initial tMWCNT or rMWCNT pulmonary exposure. A) Trichrome-stained lung sections are imaged here depicting terminal bronchioles (TB). Arrows indicate fibrotic foci (scale bars equal 200 µm). B) Relative average µg of soluble collagen per mouse lung as determined using the Sircol assay (*$p<0.05$ between genotypes). Number in parentheses above graph bar indicates number of animals per group.